Mon. Not. R. astr. Soc. (1984) **210**, 463–477

A dedicated echelle spectrometer for the Anglo-Australian Telescope

J. Meaburn, B. Blundell, R. Carling, D. F. Gregory and D. Keir *Department of Astronomy. The University, Oxford Road, Manchester M13 9PL*

C. G. Wynne *Royal Greenwich Observatory, Herstmonceux Castle, Hailsham, East Sussex BN27 7RP*

Accepted 1984 March 20. Received 1984 March 15; in original form 1984 February 1

Summary. An echelle spectrometer has been manufactured for use combined with the image photon counting system (IPCS) on the Anglo-Australian Telescope. This instrument employs a collimator/camera lens and in its principal configuration uses broad interference filters to isolate separate echelle orders. Very long multi-slits or multi-image masks can cover large areas of extended sources to obtain profiles of single emission lines, or interstellar absorption lines, from many spatial elements simultaneously. Provision is made for a grism to be inserted to achieve cross-dispersion with a short slit or, when rotated by 90°, produce a simple low dispersion spectrum of the source. Furthermore, the insertion of a plane mirror produces a direct image of the field when a clear area is driven into position to replace the multi-slits. All complex operations are remotely controlled with a BBC microcomputer.

1 Introduction

Many astronomical echelle spectrographs have been manufactured (for example, Schroeder & Anderson 1971; Learner 1972; Butcher 1971, 1975) which employ cross-dispersion and predominantly reflection optics. These devices detect light in a large number of high resolution spectral elements simultaneously. Also, because of the large blaze angles of the echelle gratings, they can have wide slits at a particular spectral resolution and, with reflection optics, can perform anywhere within a wide wavelength range. A consequence of these properties is that their principal application is to the investigation of single, faint sources of small angular diameter, which emit light over an extensive spectrum.

In contrast, an echelle spectrograph has now been made, for combination with the image photon counting system (IPCS) (Boksenberg & Burgess 1973), and the Anglo-Australian Telescope (AAT), for optimum performance on problems which require the detection of faint light in many spatial elements simultaneously, within very small wavelength ranges but at high spectral resolution. This is achieved, without cross-dispersion, by isolating individual

echelle orders with broad, efficient, interference filters and by employing predominantly transmission optics. A very long multi-slit, or multi-image mask, can then cover a large fraction of an extensive emission line or continuous source. Profiles of emission lines or absorption lines can then be obtained from large numbers of spatial elements simultaneously. (See Wilson *et al.* 1959, for use of multi-slits with a Coudé, low order spectrograph.)

Cross-dispersion, direct-field imagery and low dispersion capabilities have been included only as secondary options.

2 Optical, mechanical and electronic layout

The optical layout and various modes of operation of this echelle spectrometer are shown in Fig. 1(a–c) and the completed instrument, without IPCS, in Plate 1. A summary of the essential optical parameters is given in Table 1. The values for the multi-slits and grisms are only for the first options that have been implemented. Many more are possible.

In the first mode (Fig. 1a) a lens which is composed of two separated cemented doublets (see Section 3(f) for its detailed design) both collimates the *f*/7.9 beam from the Ritchey–Chrétien focus of the AAT, and refocuses it, after dispersion by the echelle grating, on to the 4-cm diameter photocathode of the IPCS, two-dimensional, photon-counting detector. Here a three-period interference filter isolates one order of the echelle. These filters have square profiles (see Macleod 1969, for an explanation) and half power bandwidths equal to the separation of the echelle orders which are listed versus wavelength in Table 2, for this grating with a 63° 26′ blaze angle, 31.6 groove/mm and for an angle of 3.3° between the input and output optical axes (centre of slit-assembly to centre of detector area).

A conventional slit assembly is dispensed with in this design. Single long slits, long multi-slits or multi-image masks are produced by depositing chromium on to a thin glass substrate.

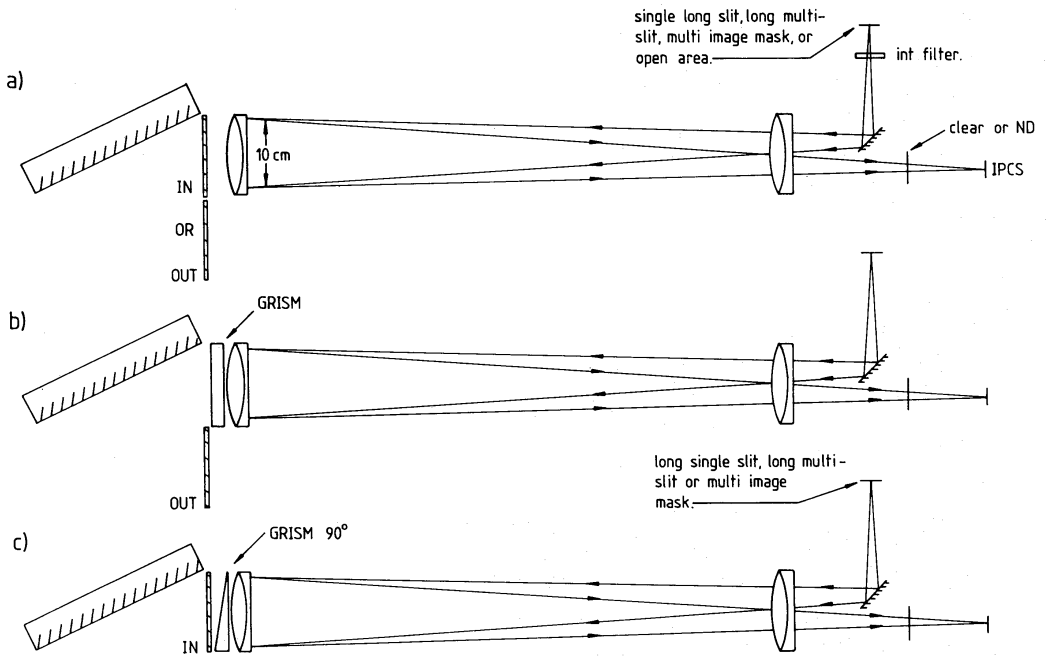

Figure 1. The various modes of operation and optical layout (to scale) of the echelle spectrometer are illustrated. In (a) an echelle order is isolated by an interference filter or, with the excluding mirror in, a direct image of the field is formed. In (b) a grism cross-disperses the echelle orders, and in (c) the same grism, rotated by 90°, with the mirror in, forms a low dispersion spectrum.

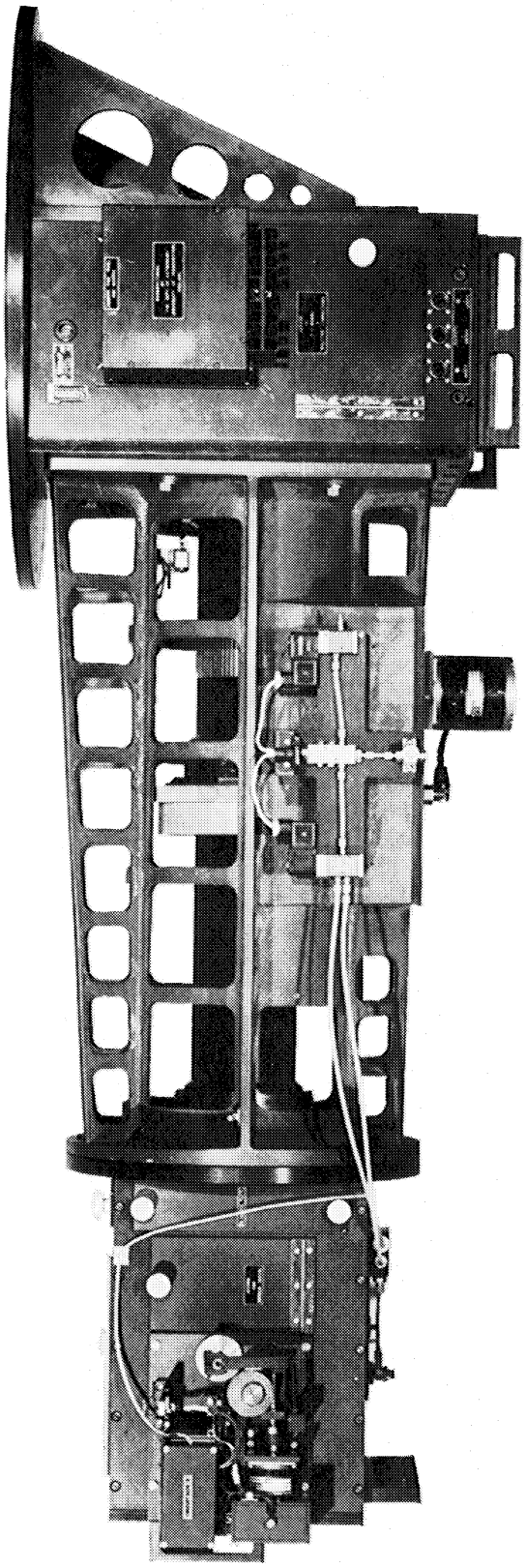

Plate 1. The echelle spectrometer after manufacture. IPCS, which is not shown, bolts on to the right-hand side.

[*facing page* 464]

Table 1. A summary of the parameters of the dedicated echelle.

ECHELLE GRATING
(Bausch and Lomb)

Blaze angle	Grooves/mm	Dimensions of ruled area
63°26'	31.6	128 x 254 mm

SPECTROMETER

Beam diam.	Focal length	Angle between central input and output beams
100 mm	800 mm	3.3°

Anti-reflected Wavelength Range (TRIOLIN)
3900 - 7500 Å

MULTI-SLITS

	Length (mm)	Separation	Width (microns)		
	30	3.3 mm	70	150	600
a) Five element	(≡ 3.4')	(≡ 22.4")	(≡ 0.47")	(≡ 1.00")	(≡ 4.03")
		(≡ 292kms^{-1})	(≡ 6kms^{-1})	(≡ 13kms^{-1})	(≡ 53kms^{-1})
b) Three element	"	6.6 mm	"	"	"
		(≡ 44.8")	"	"	"
		(≡ 584kms^{-1})	"	"	"

FIELD AREA

25 x 30 mm
(≡ 2.8' x 3.4')

MAX SPECTRAL RESOLUTION $\lambda/\delta\lambda$

10^5 for 30 micron pixels

Table 2. Dispersion and separation of orders for the echelle for blaze angle 63° 26′, 31.6 grooves mm^{-1}, 800 mm focal length and 3.3° between input and output optical axes.

Wavelength (Å)	Dispersion (Å/mm)	Separation of adjacent orders (Å)
4000	1.32	28
4500	1.49	36
5000	1.65	44
5500	1.82	53
6000	1.98	63
6500	2.15	75
7000	2.31	86
7500	2.48	99

The maximum slit length is 30 mm (= 3.4 arcmin) and the separate slits are placed anywhere within a 25 mm (= 2.8 arcmin) width in the common focal plane. A variable 'decker' can be moved over the slit area to change for example a five-slit multi-slit into a three-slit one but with greater separation between the adjacent slits (see Table 1).

A multi-image mask, which is composed of a number of short slits, which are pre-arranged to cover many separate sources within this field, can also be used. In addition, with the plane mirror in and an open area replacing the various slits, a direct, filtered image of the field can be formed.

A variety of neutral density filters are always required (see Fig. 1) with IPCS to diminish the intensity of sources which produce signals much in excess of 3 counts $\text{pixel}^{-1}\,\text{s}^{-1}$.

The slit area can be evenly illuminated with light from copper–argon or helium emission line lamps, for spectral calibration, or a tungsten white light source for flat fielding.

It is also possible (see Fig. 1b) to produce a cross-dispersed echelle spectrum by the insertion of a grism (see Section 3(e) for detailed design) and the extraction of the filter. Furthermore, a low dispersion spectrum of a source which illuminates the slits can be obtained (see Fig. 1c) by inserting the plane mirror and rotating the same grism by 90°.

For maximum efficiency all air/glass transmission surfaces have been coated with broadband, Triolin, anti-reflection layers. Between 3900 and 7500 Å each transmission then only loses 0.5 per cent of the incident light.

In the principal mode (Fig. 1a) there are 12 such transmissions, consequently only 6 per cent of the light is lost at these interfaces. At wavelengths longer than 7500 Å these coatings become ineffective and the losses revert to approximately 4 per cent per transmission in

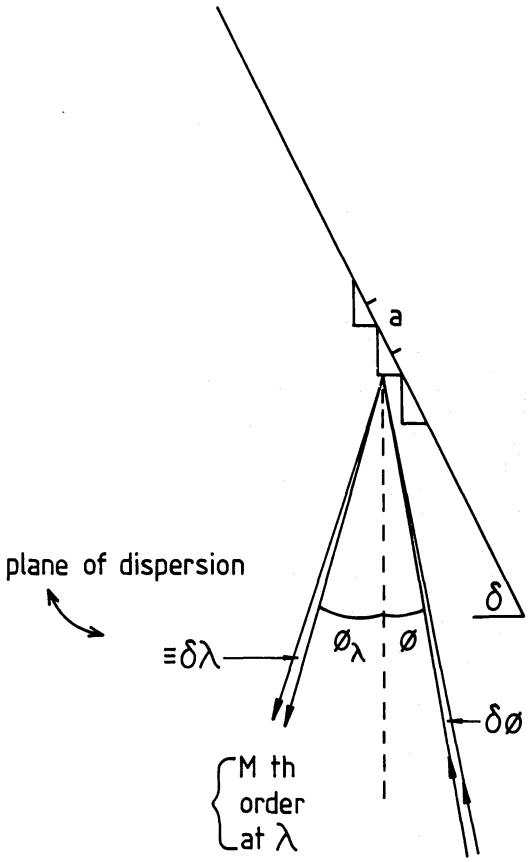

Figure 2. The parameters of an echelle grating are shown. A position along a long slit subtends an angle θ to the echelle in a plane perpendicular to that of the dispersion.

which case, overall, 34 per cent is lost for this reason alone. Below 3900 Å these same layers start to become enhanced reflection layers and the spectrometer has no application within that wavelength domain. The flint glass in the lenses also absorbs light heavily at wavelengths shorter than 3700 Å.

Both reflecting mirrors shown in Fig. 1 have enhanced reflection coatings (> 95 per cent reflection) and can be easily replaced with newly deposited ones before each observing run.

The imagery of the lens, and the linear resolution of the IPCS in the direction of the dispersion, permit elements of the field that are separated by $\gtrsim 30\,\mu$m to be resolved. The maximum spectral resolution of the echelle in Table 1 is based on this value.

Most of the operations are remotely controlled with a BBC microcomputer in which the control program is permanently stored in EPROM. The control signals are passed down twisted pair lines to the driver cards which power the stepping motors on the spectrometer. Any of three options for the slit assembly and four for the colour filters (moved by linear Geneva mechanisms (Yeaple 1979)) are selected in this way. So too is the rotation of the echelle grating, focusing of the lens and the selection of any of six positions in the rotating neutral density wheel (ND = 0–2).

Both the in/out mirror (see Fig. 1) and the illuminating mirror for the calibration lamps are pneumatically moved by separate, remote, manual switches. The grism is manually inserted (see Fig. 1b, c). A separate manual switch remotely operates the safety shutter immediately in front of the IPCS cathode.

A rotation of the grating (changing δ in equation (1)) of 10^{-3} degrees changes the position of the spectrum on the photocathode by 30 μm. The spectrometer must then be sufficiently rigid to prevent this motion occurring through flexure at any orientation of the whole device. The casting which separates the grating holder from the slit/filter box (see Plate 1) was designed to be 10 times more rigid than this minimum requirement.

3 Detailed optical considerations

(a) MAXIMUM SLIT WIDTH

For an echelle spectrograph, at a given spectral resolution, $R = \lambda/\delta\lambda$, where $\delta\lambda$ is the half-width of the response to an infinitely narrow emission line of wavelength λ, the maximum angular slit width, $\delta\phi$, should be aimed for in the design. This permits the greatest amount of light to be detected in each spectral element.

For the case in Fig. 2 where the incoming beam, from the centre of the long slit, is incident at ϕ to the optical axis and the mth order of wavelength λ is at ϕ_λ to the axis then with a blaze angle, δ, and groove separation, a,

$$m\lambda = a\{\sin(\phi + \delta) + \sin(\delta - \phi_\lambda)\}. \tag{1}$$

For the case where $\phi = \phi_\lambda$, from the differentiation of equation (1),

$$R\,\delta\phi = 2 \sin\delta \cos\phi/\cos(\delta - \phi). \tag{2}$$

To maximize $R\,\delta\phi$ the value of δ should be as large as possible and ϕ should tend to zero. For echelle gratings δ can have a value of 75° but here one with $\delta = 63°\,26'$ was chosen to permit full use of a 100 mm beam diameter (see Table 1). For multi-slits, the field area has to be substantial and the minimum value of ϕ that is possible in the present design is 1.65°. In this case $R\,\delta\phi = 3.79$ rad compared with a value of 4.00 if ϕ had been zero.

(b) OPTICAL EFFICIENCY

The optical transmission efficiency ϵ_S of this spectrograph is given by

$$\epsilon_S = \epsilon_E \epsilon_F \epsilon_R \epsilon_A \epsilon_{AG}^N \epsilon_V \epsilon_O \tag{3}$$

where the efficiency ϵ_E of the echelle grating is 0.75. That of the interference filter ϵ_F is 0.85, of the high reflectance mirror ϵ_R is 0.95 and $\epsilon_A \cong 0.90$ is introduced by the absorption in the thick glasses of the lenses between 4000 and 7500 Å. For the outer surfaces of the interference filter and a double passage through the lenses there are reflection losses at 12 air/glass ($N = 12$) surfaces. All of these are anti-reflected therefore the transmission efficiency introduced by these becomes $\epsilon_{AG}^N \cong 0.94$. The vignetting along the slit length and the loss that can arise if the beam overfills the grating is represented in equation (3) by ϵ_V. In the present design the component of the collimating/camera lens nearest the slit forms an exit pupil on the centre of the grating. Also, as can be seen from Table 1 and Fig. 1 the grating is sufficiently large to intercept all of the 100 mm beam. In this case, negligible vignetting occurs, therefore $\epsilon_V \cong 1$ in equation (3). The component of the transmission efficiency ϵ_O is introduced in equation (3) to represent the reduced efficiency if a particular wavelength does not fall at the peak of the blaze transmission (where $\phi = \phi_\lambda$ in Fig. 2) for a particular order m in the mode shown in Fig. 1(a). Values of ϵ_O are anywhere between 0.5 and 1 for a random wavelength.

The values of ϵ_O, for a single slit, with this value of $\phi = 1.65°$, for this grating with 31.6 grooves mm^{-1} and $\delta = 63° 26'$, for the rest wavelength of many nebular emission and absorption lines, are indicated in Fig. 3. The Doppler shifted values of these wavelengths will have significantly different values of ϵ_O.

However, for a wavelength where $\epsilon_O = 1$ this spectrograph has an overall efficiency $\epsilon_S \cong 0.51$ which is very high. Furthermore, if the grating is well protected, ϵ_S does not degrade with time as can a spectrometer with ageing reflection optics.

There are two ways of making $\epsilon_O = 1$ for any wavelength. The first possibility is to immerse the echelle grating in a gas which has a high change of refractive index with change in pressure (ΔP atmospheres). Here the wavelength at a particular angle out, ϕ_λ, also changes by $\Delta\lambda_s$ but the peak of blaze efficiency still remains in the same place if the condition is satisfied that $\phi = \phi_\lambda$.

As shown for the gratings in a SISAM monochromator (Meaburn 1973)

$$\Delta\lambda_s = k\,\Delta P\,\lambda \tag{4}$$

where k is a constant characteristic of the immersing gas. A particular wavelength to the short side of the blaze maximum ($\epsilon_O = 1$ in Fig. 3) can then be scanned towards this position by increasing the gas pressure. Woolf (1959) discovered that propane has a high value of $k = 0.0011\ atm^{-1}$. In which case, for a pressure increase of $\Delta P = 8$ atm (the liquefying point of propane) a change $\Delta\lambda_s \cong 44$ Å of the wavelength emerging at a particular ϕ_λ occurs. This is equivalent to the value of the separation of adjacent orders in Table 2 at 5000 Å.

However, the weight of the chamber that is required to withstand this high pressure in the present design was considered prohibitive. In any case an alternative method can have some effect.

For any given wavelength an echelle has its maximum efficiency ($\epsilon_O = 1$) for equal input and output angles ($\phi = \phi_\lambda$ in Fig. 2 and equation (1)).

The values of ϕ and ϕ_λ which satisfy this condition between 4940 and 5100 Å, for various integer values of m in equation (1), are shown in Fig. 4 for this particular echelle grating. It can be seen that an ability to change $\phi = \phi_\lambda$ over a range of 8° is necessary to bring any wave-

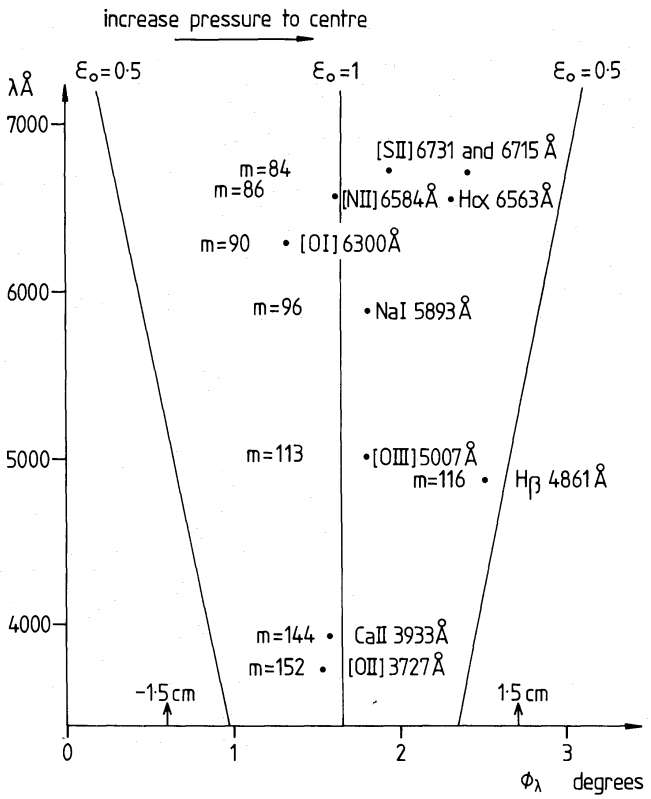

Figure 3. The output angles ϕ_λ for the spectra of various rest values of useful nebular lines are shown for the centre of a long input slit in the configuration in Fig. 1(a), with the parameters in Table 1 ($\phi = 1.65°$ and $\theta = 0°$). A 3 cm length across the IPCS cathode is indicated as are the 0.5 efficiency positions along echelle orders.

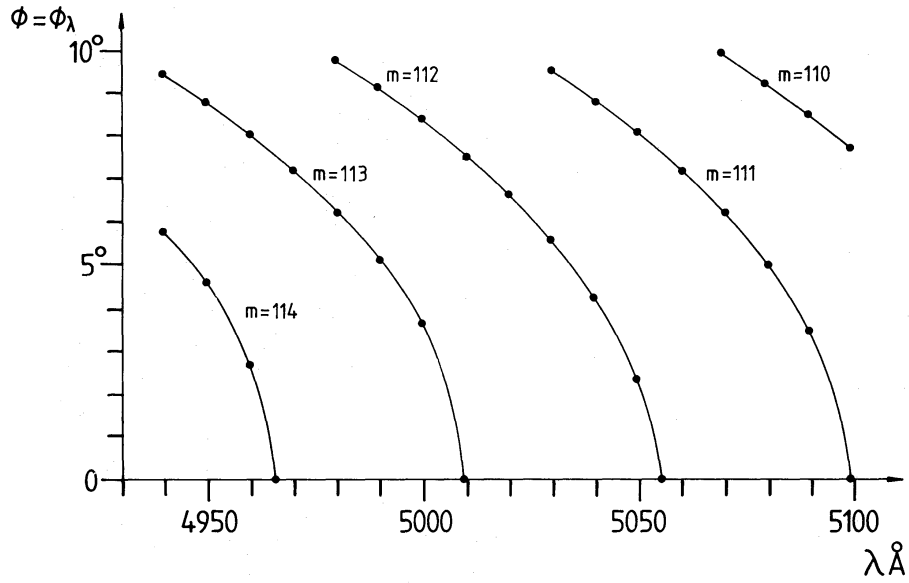

Figure 4. Curves of maximum efficiency ($\epsilon_O = 1$) along echelle orders, m, for equal input and output angles ($\phi = \phi_\lambda$) for the configuration in Fig. 1(a) and parameters in Table 1.

length in Fig. 4 on to the blaze maximum, though note the penalty predicted by equation (2) of increasing ϕ to this extent ($R\delta\phi$ would decline to 3.12). Values of ϕ and ϕ_λ of 8° correspond to a width of 11 cm in both the slit area and over the photocathode in the present instrument which is prohibitively large. However, judicious selection of the grating parameters, combined with the significant ranges of ϕ and ϕ_λ that are available in the design (2.5 cm is the width of the slit area and 4 cm that of the photocathode) permits many wavelengths (see Fig. 3) which are very useful for studies of the interstellar medium to be observed with $\epsilon_O \cong 1$ in equation (3). In a future design it is conceivable that pressure scanning could be combined with a limited ability to change ϕ and ϕ_λ to achieve $\epsilon_O \cong 1$ for any wavelength.

(c) LONG MULTI-SLITS

Many problems associated with the interstellar medium require profiles of single emission lines from a large number of small, separate areas of faint extensive sources. Consequently, it is desirable to transmit the light simultaneously through many separated entrance slits which are each as long as possible for astronomical problems of this nature.

In the present instrument the length of the entrance slit is maintained on the photocathode and 3 cm is about the maximum attainable for this parameter. For a slit as long as this, a significant curvature occurs in the output spectrum.

Equation (1) is now replaced by

$$m\lambda = a\cos\theta\{\sin(\delta+\phi)+\sin(\delta-\phi_\lambda)\} \tag{5}$$

and then

$$\phi_\lambda = \delta - \sin^{-1}\left\{\frac{m\lambda}{a\cos\theta} - \sin(\delta+\phi)\right\} \tag{6}$$

where θ is the angle away from the spectrometer's optical axis, of a position along a long slit, in the plane perpendicular to that of the dispersion (see Fig. 2).

The linear curvature, δx, of the output spectrum, when monochromatic light of wavelength λ illuminates a long, single, entrance slit, is given by

$$\delta x \cong f\frac{\pi}{180}\left\{\phi_\lambda(\theta) - \phi_\lambda(\theta = 0^\circ)\right\} \tag{7}$$

where f is the focal length of the collimating/camera lens (see Table 1) and $\phi_\lambda(\theta)$ and $\phi_\lambda(\theta = 0^\circ)$ are the values of the output angles in equation (6) for θ and $\theta = 0^\circ$ respectively.

This curvature, for a monochromatic line at 5007 Å illuminating the straight entrance slit of 30 mm length (for $\phi = 1.65^\circ$, $\delta = 63^\circ 26'$ and $m = 113$ – see Table 1) is shown in Fig. 5. The amount of curvature is relatively insensitive to wavelength and input angle ϕ over the ranges of these parameters encountered in this spectrograph.

When used with IPCS, 'pin-cushion' distortion is added to this intrinsic curvature; consequently a technique for wavelength calibration has to be devised to compensate for the combination of these effects. This problem is further complicated when a multi-slit is being used, over a small wavelength range, for often only one bright lamp line, of known wavelength, is available.

This difficulty can be overcome if the parameters of the multi-slit are known to a sufficient degree of accuracy. For the present ones, slit separations are 3.30 ± 0.01 mm. Therefore it is possible to predict the output angle, ϕ_λ, from equation (6) for the slit centre ($\theta = 0^\circ$) for each of the input angles, ϕ, of the slits. When this has been obtained, ϕ_λ can be inserted into equation (5) to predict the equivalent wavelength out as though only a single central slit

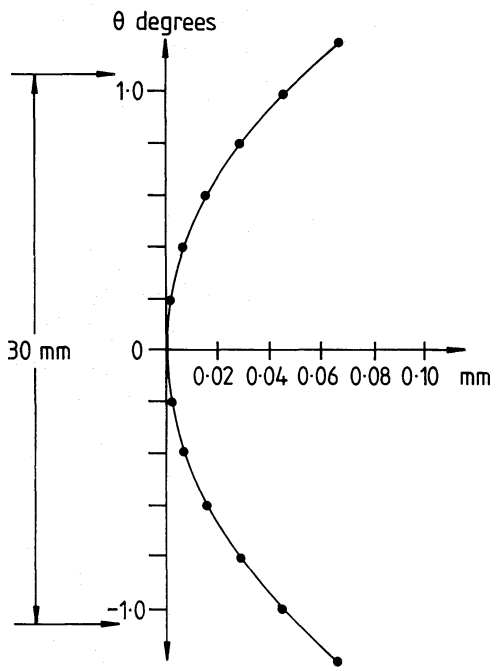

Figure 5. The curvature of the spectrum at 5007 Å for a 30 mm long slit is depicted for an input angle $\phi = 1.65°$ and the echelle parameters in Table 1.

were being used, with $\phi = 1.65°$ from this spectrograph. This procedure is illustrated in Table 3 for these five multi-slits, illuminated by the He I 5016 Å line and used in the order $m = 113$.

The values in column 4 of Table 3 can be used to simulate separate emission lines as though the multi-slit were a single slit. The output spectrum can now be 'scrunched' in the computer to eliminate all curvatures and calibrate the spectrum. As the IPCS also introduces a non-linearity in the direction of dispersion a second or third order polynomial must be used to obtain the calibration coefficients used in this procedure. A by-product of this process is apparent in column 5 of Table 3. It can be seen that the equivalent wavelength separation of adjacent multi-slits is a significant function of the input angle ϕ given in column 2. Only the mean values for each multi-slit (converted to km s^{-1}) are presented in Table 1. This illustrates that a detailed calculation has to be performed for each configura-

Table 3. The equivalent wavelengths out, for order $m = 113$ of a multi-slit, illuminated by the He I 5015.68 Å line. The values in column 4 are for $\phi = 1.65°$ combined with the values of ϕ_λ in column 3 in equation (5). The slit separations are 3.3 mm.

1	2	3	4	5
Slit	Input angle ϕ	Output angle ϕ_λ for 5015.68 Å	Equivalent wavelength out for ϕ = 1.65°	Equivalent separation of adjacent slits
	degrees	degrees	Å	Å
1	2.123	1.714	5006.03	
				} 4.81
2	1.886	1.506	5010.84	
				} 4.84
3	1.650	1.295	5015.68	
				} 4.89
4	1.414	1.080	5020.57	
				} 4.93
5	1.177	0.862	5025.50	

tion to be sufficiently precise in the analysis of real data. Incidentally, a Th–Ar lamp may emit sufficient lines (Burenkov *et al.* 1980; Chaffee & Peters 1983) to provide many in any wavelength range, which would simplify this calibration procedure. However, this has not been tested.

(d) A TWICE-THROUGH GRISM AS A CROSS-DISPERSER

It is shown in Fig. 1(b) that a grism, in which the light is passed twice through, can act as a cross-disperser. A grism (see Bausch & Lomb, 1970) is a blazed transmission grating, with groove angle γ, and groove separation a, which, when placed on a prism of refractive index $\mu(\lambda)$ and angle γ, has its blaze wavelength, λ_B, along the axis perpendicular to its back face. Its use as a twice-through cross-disperser is shown in Fig. 6. Here, for an order, m,

$$m\lambda_B = a \sin\gamma\{\mu(\lambda_B) - 1\}, \tag{8}$$

$$\beta = \sin^{-1}\{\mu(\lambda)\sin\gamma - m\lambda/a\} \tag{9}$$

and

$$\eta = \sin^{-1}\left[\mu(\lambda)\sin\left\{\sin^{-1}\left(\frac{1}{\mu(\lambda)}\{\sin(2\gamma-\beta)\} + \frac{m\lambda}{a\mu(\lambda)}\right) - \gamma\right\}\right]. \tag{10}$$

The behaviour of a grism as a cross-disperser over large wavelength ranges is complicated by the change of the refractive index of glass with wavelength. Practical grisms can be made which would perform usefully in this role for this spectrograph. Their performances, derived from equations (8)–(10) and assuming a focal length of 800 mm (see Table 1) are listed in Table 4. Their surfaces could be anti-reflected to diminish their transmission losses (ϵ_G now replaces ϵ_F in equation (3)).

The first grating in Table 4 which has a blaze wavelength of 5230 Å and $\cong$ 83 Å mm^{-1} dispersion will produce, in one IPCS frame, from $\cong$ 3900 to $\cong$ 6000 Å of cross-dispersed spectrum. It can be seen in Table 2 that complete echelle orders for wavelengths $\lesssim$ 6000 Å can be accommodated in the 3 cm width of an IPCS window; though at 4000 Å adjacent orders will only be separated by $\cong$ 0.35 mm with this cross-disperser. This is equivalent to

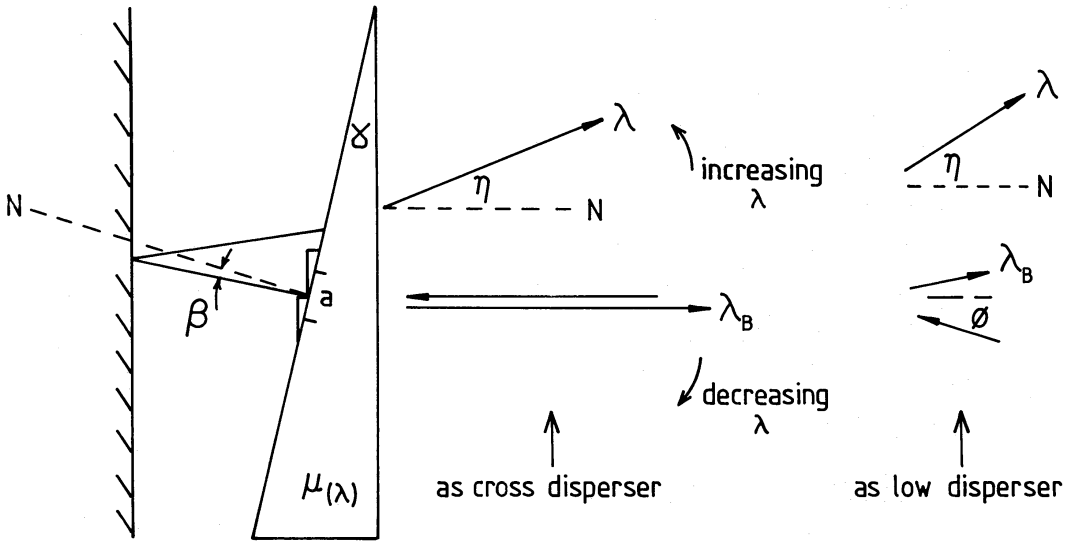

Figure 6. The parameters of a grism used as a twice through cross-disperser in the configuration in Fig. 1(b) and as a low-dispersion element in Fig. 1(c) are shown schematically.

Table 4. Practical, twice through, grisms as cross-dispersers.

Order m	Angle γ	Grooves/mm	Refractive Index $\mu(\lambda_B)$	Blaze wavelength λ_B Å	Dispersion Å/mm (at λ_B)
1	4°18'	75	1.523	5230	83
1	8°38'	150	1.523	5230	41
1	10°48'	150	1.515	6430	41

only 2.3 arcsec on the sky, and a very short slit, with no room for simultaneously detecting the sky background, would have to be used. Incidentally, the refractive indices $\mu(\lambda)$ of BSC-7 glass for the prism at 4000 and 6000 Å are 1.531 and 1.513 respectively. These are very nearly the same as those of the material of the replica grating cemented to its sloping surface. Consequently, using equation (10) combined with a focal length of 800 mm, the dispersions at these two extreme wavelengths will be 82.6 and 83.3 Å mm^{-1} respectively, which is not a large difference.

(e) THE GRISM AS A TWICE THROUGH LOW DISPERSER

The possibility of obtaining a low dispersion spectrum of the source which illuminates a long, single or multi-slit is also illustrated in Fig. 1(c). Here the same grism as described in Section 3(d) for cross-dispersion is rotated by 90° and the plane mirror is inserted which eliminates the echelle. The behaviour of the grism is now modified to some extent for the incoming beam is at an angle ϕ (in the plane of its dispersion) to the normal of the back face of the grism (see Fig. 6). In this case equations (8) and (9) are replaced respectively by

$$m\lambda_B = a\left[\mu(\lambda_B)\sin\left\{\gamma - \sin^{-1}\left(\frac{(\sin\phi)}{\mu(\lambda_B)}\right)\right\} - \sin(\gamma - \phi)\right] \tag{11}$$

and

$$\beta = \sin^{-1}\left[\mu(\lambda)\sin\left\{\gamma - \sin^{-1}\left(\frac{(\sin\phi)}{\mu(\lambda)}\right)\right\} - \frac{m\lambda}{a}\right] \tag{12}$$

and equation (10) remains the same.

For the gratings in Table 4 the value of λ_B given by equation (11) only changes by $\cong 1$ Å for such a small value of $\phi = 1.65°$ and the dispersions are practically identical to those listed though the angle, η, is now different at any particular wavelength.

(f) DESIGN OF COLLIMATING/CAMERA LENS

A refracting camera–collimator system has several advantages over the reflecting cameras and collimators more commonly used in astronomical spectrography; in particular it leads to a more compact instrument with the echelle working nearer to the Littrow configuration. But mirror systems are generally preferred because of the chromatic aberrations inherent in lens systems, which become serious when a wide spectral range is to be covered. These aberrations fall into two groups. There is the secondary spectrum defect, arising from a mis-match between the rate of change of refractive index with wavelength for crown and flint glasses, which produces a residual change of focal position with wavelength, even for so-called achromatic systems. In addition, lens systems generally show a rather large change with wavelength of their other aberrations.

The combined collimator camera used in double-pass in this spectrograph is a Petzval lens system, consisting of two close doublet lenses, rather widely separated. It is well known that this configuration can be designed to give a high level of correction of spherical aberration, coma, and astigmatism over the field angles required in this spectrograph over a curved focal surface. Further, by appropriate choice of the optical glasses used, this can be achieved using separated cemented doublets, thus reducing the number of air–glass surfaces. It has been found possible to combine these features with an aberration correction that is almost invariant with wavelength over the wide spectral range required. Thus while the system shows the normal secondary spectrum change of focal position, it can give high resolution imagery over a wide spectral range provided narrower sections of this range are recorded separately, with appropriate refocusing. This accords with the requirements of this echelle spectrograph in its primary mode where filters are used to isolate different spectral regions. Over the range 3900–7000 Å, the range of change of focus is 3.2 mm. In the low dispersion mode or with a cross-dispersed echelle spectrum, over wavelength ranges of $\gtrsim 1000$ Å, slit widths $\gtrsim 60$ μm must be used. Alternatively the detector could be tilted to match the focal surface at different wavelengths or a field flattening wedge placed before the neutral density filter shown in Fig. 1(b, c).

The focal surface of the system at any wavelength is curved, with a radius of 77 cm. With this large radius of curvature, it is possible to tilt plane multi-slits and detector so that the ends and middle of the spectrum are equally, and negligibly, defocused.

4 Performance

The performance in the laboratory of the spectrograph, in the configuration shown in Fig. 1(a), is illustrated in Plates 2(a, b). Plate 2(a) shows a direct polaroid image of the five-element multi-slit illuminated by the Cd 6438 Å line. Each slit is 30 mm long and 70 μm wide and separated by 3.3 mm from its neighbours. This was obtained with the flick mirror, shown in Fig. 1(a), in a position which excludes the echelle grating. The edges of the images of these slits were scrutinized with a high-power, wide-field, Erfle eyepiece and found over the whole field to be sharp in comparison with their 70 μm width. This illustrates that the collimating/camera lens is working well within its specification for $\lesssim 30$ μm imagery.

The polaroid in Plate 2(b) is with the flick mirror removed and shows the spectrum produced by the same five slits. The polaroid camera introduces no distortion and the curvature that is predicted in Section 3(c) (see Fig. 5) is apparent.

This particular image is the superposition of two separate exposures. The first was taken with the spectrograph suspended at both extremes and the second when suspended only at its centre of gravity. This represents an extreme test for mechanical flexure in the main casting (see Section 2), for any bending would occur in the direction of the dispersion. No displacement of the profiles $\gtrsim 30$ μm was observed which confirms the rigidity of this design.

On the telescope small shifts in the positions of the profiles of emission lines were produced by the changes occurring within IPCS as the orientation of the instrument changed. In the worst case these amounted to $\simeq 1$ pixel (30 μm) for a change of right ascension of 1 hr. Frequent calibration exposures (every 0.5 hr) eliminate any significant errors of this origin during very long integration times.

The images in Plates 3(a, b) were obtained with the spectrograph combined with the Anglo-Australian Telescope and with IPCS as the detector. Here a multi-slit with three elements (a 'decker' masked two of the elements in a five-element array – see Table 1) was used. Each slit is 30 mm long ($\equiv 3.4$ arcmin on the sky) and 150 μm wide ($\equiv 1$ arcsec).

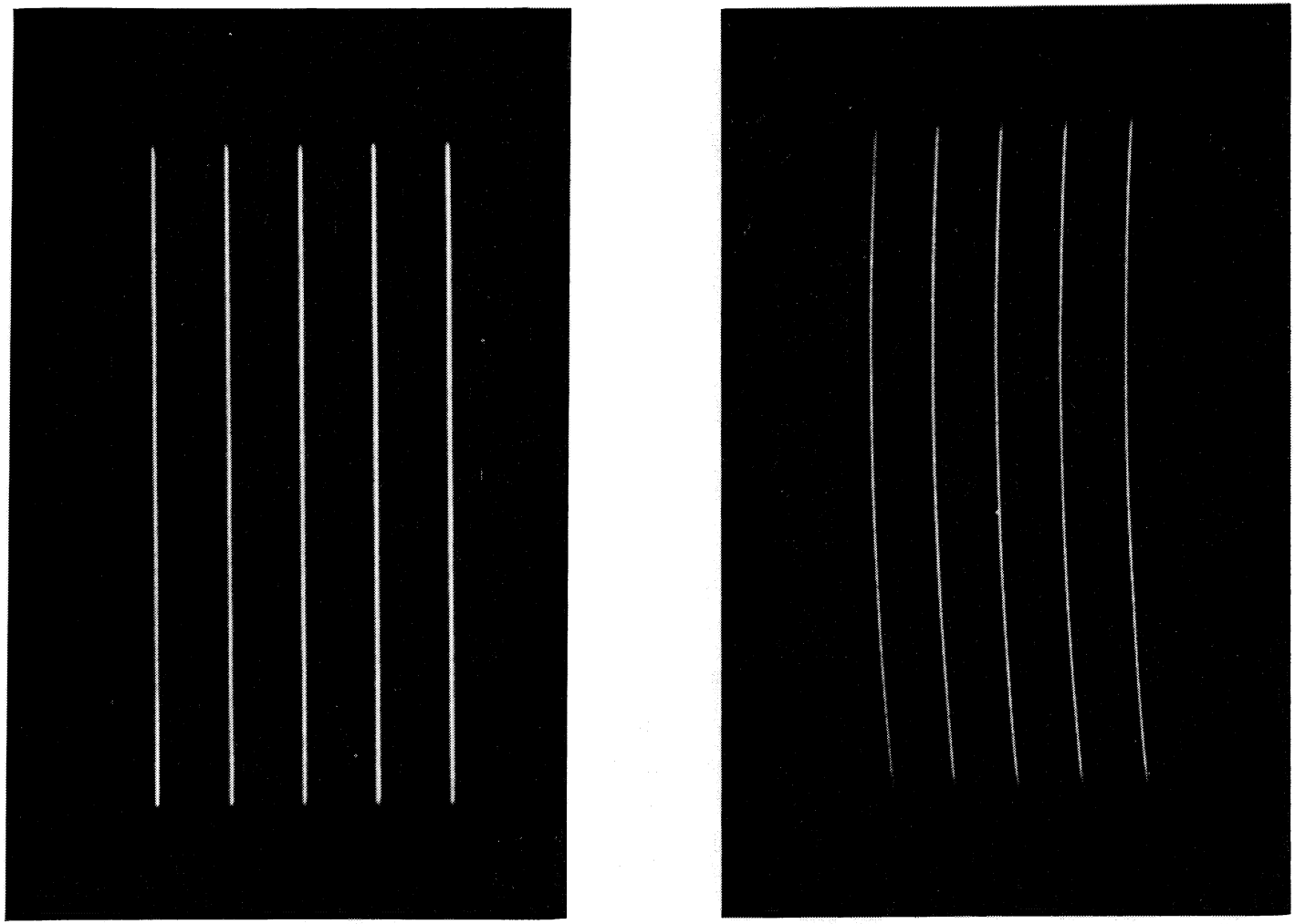

(a) (b)

Plate 2. (a) A polaroid of the five element multi-slit (width 70 μm) illuminated by the Cd 6438 Å line, taken with the excluding mirror in, as shown in Fig. 1(a). (b) The profiles of the Cd 6438 Å line with the same multi-slit but with the excluding mirror out in Fig. 1(a). This was obtained on polaroid during a laboratory load test.

[*facing page 474*]

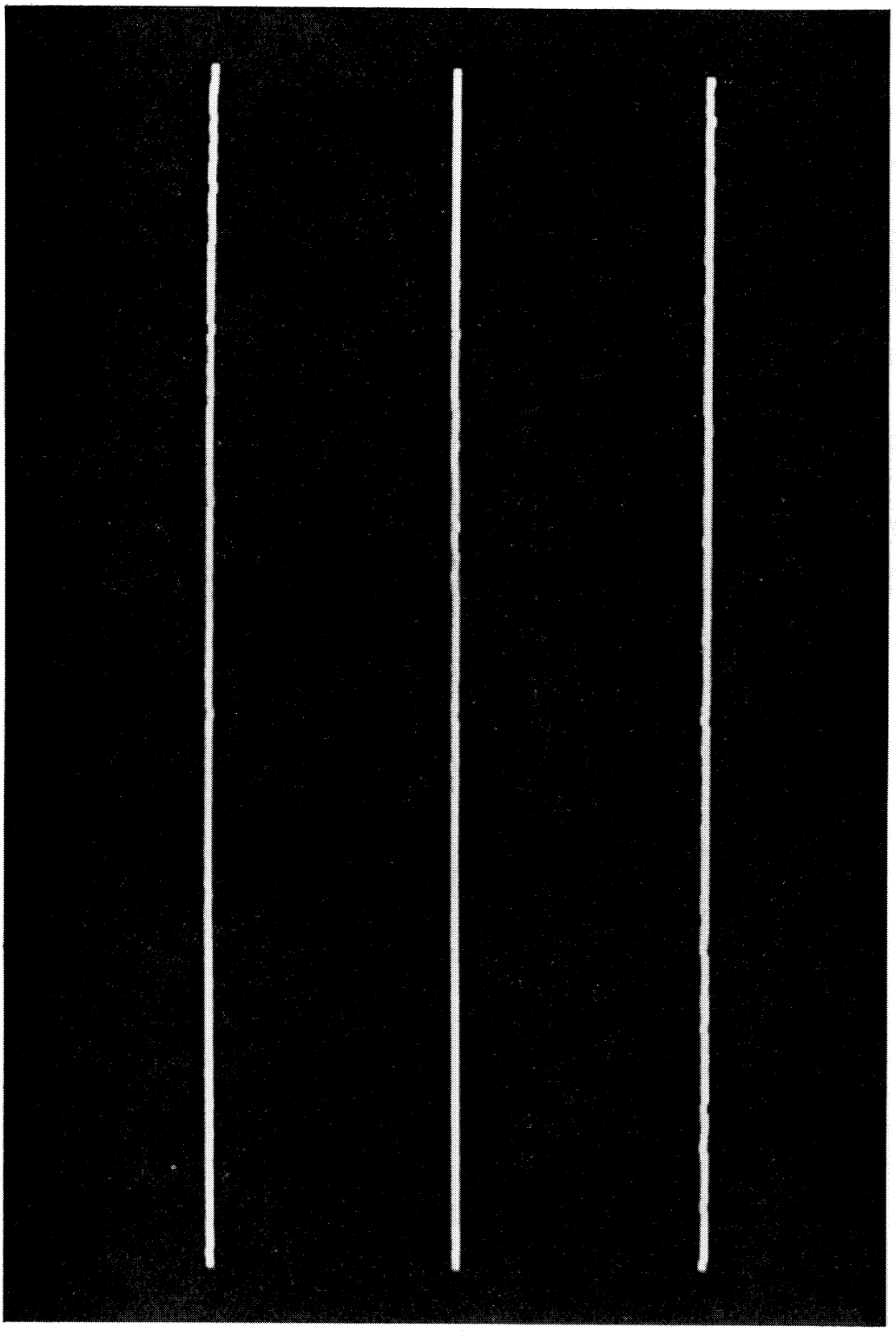

Plate 3(a). The profiles of the calibration He I 5015.68 Å lamp line obtained with a three-element multi-slit of width 150 μm after correction for curvature and distortion. The detector was IPCS.

Plate 3(b). The profiles of the [O III] 5007 Å nebular line from the edge of a giant shell in the LMC obtained with a three-element multi-slit in the configuration shown in Figure 1(a). These have been corrected for distortion and curvature and calibrated in wavelength with the lamp profiles in Plate 3(a). The detector was IPCS.

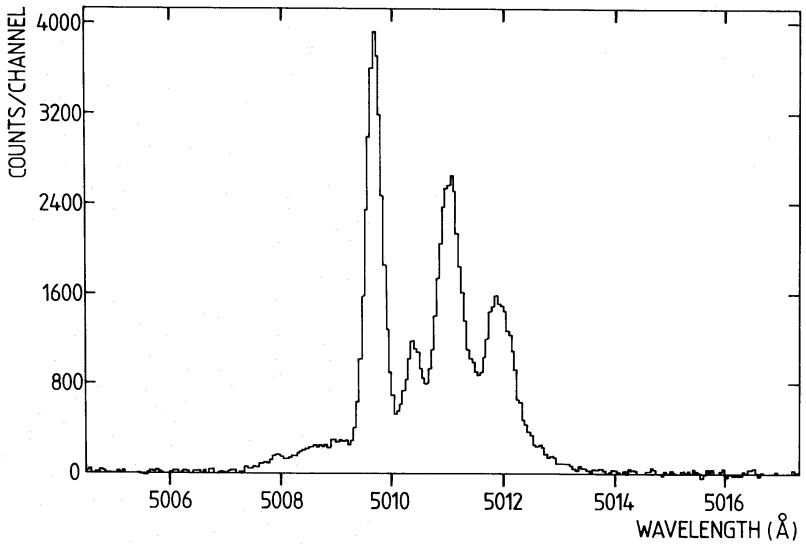

Figure 7. The complex profile of the [O III] 5007 Å line from the centre of the middle slit in the data array shown in Plate 3(b).

One hundred and twenty data-taking windows, each 250 μm long, were placed along the slit lengths and 1020 30-μm windows along the direction of dispersion. The data array illustrated in Plate 3(a) was produced by the He I 5015.68 Å lamp line and was used to calibrate that in Plate 3(b) which shows the profiles of the [O III] 5006.85 Å nebular emission line from part of a giant shell (Meaburn 1980) near the 30 Doradus nebula.

The curvatures produced by long slits (see Fig. 5 and Plate 2b) and the additional distortions introduced by IPCS have been removed in both of these data arrays by the method described in Section 3(c).

These images were photographed off an ARGS screen after processing with the VAX 780 computer of the Manchester node of the STARLINK network. The image in Plate 2(b) shows only some of the complexity of the motions within this turbulent region.

The profile of the [O III] 5007 Å line through a small section of the centre of the middle slit in Plate 3(b) is shown in Fig. 7. Here many separate components in radial velocity are revealed over a range of $\cong 400\,\mathrm{km\,s^{-1}}$. In this work only three slits were used, each separated by equivalent to $\cong 584\,\mathrm{km\,s^{-1}}$ because of the large velocity range in this nebula, though note the exact calculation described in Section 3(c) that is necessary to predict this value precisely.

It can be seen in Figs 3 and 4 that the [O III] 5007 Å line, which is Doppler-shifted to $\cong$ 5012 Å in the LMC, is placed for the central slit ($\phi = 1.65°$) very nearly at the peak of the echelle transmission for order $m = 113$, in which case $\epsilon_O \cong 1$ in equation (3) for all of these observations.

Direct IPCS images, with the flick mirror excluding the echelle grating (Fig. 1a), were also successfully obtained of Seyfert nuclei through interference filters, as were many spectra of galactic H II regions with the five-element multi-slit with each slit 70 μm wide (see Table 1).

The efficiency of this echelle was demonstrated in the use of the control program ASPECT (Wallace 1983). Here the telescope steps across the sky in a direction perpendicular to the slit length and the IPCS data from each telescope position are assigned to a separate memory file. To cover the whole field the telescope need only step within the distance separating adjacent slits in the multi-slit. The time to produce a complete three-dimensional block of data (X, Y and spectral) of this whole field is then diminished by a factor equal to the number of elements in the multi-slit.

This dedicated spectrograph, in its principal configuration shown in Fig. 1(a), overlaps in its application to extensive emission line sources with several other devices; notably classical Fabry–Perot spectrographs (Courtès 1960; Meaburn & White 1982), insect-eye Fabry–Perots (Meaburn 1975; Meaburn & McMullan 1976), stepped Fabry–Perots such as 'Taurus' (Taylor & Atherton 1980; Atherton *et al.* 1982), or long-slit, low-order, spectrographs such as the intermediate dispersion spectrograph on the AAT (Palmer & Gietzen 1972). A detailed comparison of its performance relative to these will be given in a separate paper.

Realistic comparisons are very complicated in practice, for there are so many variable parameters in each instrument, and astronomical sources, even of the same type, differ from each other to such a large extent. Moreover, the information which is required about these sources covers a wide range of possibilities. In addition, observing conditions are variable and each instrument responds in a different way to the same conditions. For instance Taurus is a Fabry–Perot which steps *sequentially* through the spectral elements contained within its free spectral range. When observing extensive emission line sources this disadvantage is offset by its very wide field, particularly where line profiles are required from each spatial element within the whole field. On the other hand the dedicated echelle, when combined with an interference filter, detects light in all the spectral elements simultaneously. Consequently the echelle (with a single or multi-slit) is far more efficient than Taurus when used to obtain line profiles across extensive emission-line sources from spatial elements along long lines. Furthermore, Taurus performs badly on problems which require absorption line profiles from single or extensive continuum sources and for emission line sources superimposed on a bright continuum background. Unwanted continuous light is transmitted by all the Fabry–Perot orders within the bandwidth of the interference filter. The present echelle, with a multi-image mask or a single slit, has no such difficulty. However, when a multi-slit is used on extensive emission line sources which contain a central continuum source (e.g. a planetary nebula with a central star), the continuous light from the star contaminates all line profiles from the central elements of each slit. The insertion of a simple opaque area over the centre of the central slit to block the transmission of the starlight eliminates this problem.

Acknowledgments

We wish to thank members of the instrumentation section of the RGO for most useful advice on mechanisms for grating spectrometers. In particular we are grateful to Peter Ellis for suggesting Geneva mechanisms. Also JM and DK are grateful to the generous help received at the telescope during the first use of the instrument in November 1983, from all members of the staff there. The whole project was sponsored by grants from the SERC and JM also thanks them for his Senior Fellowship, DK his Research Studentship and BB his Post-Doctoral Research Assistantship.

References

Atherton, P. D., Taylor, K., Pike, C. D., Harmer, C. F., Parker, N. M. & Hook, R. N., 1982. *Mon. Not. R. astr. Soc.*, **201**, 661.

Bausch & Lomb, 1970. *Diffraction Grating Handbook.*

Boksenberg, A. & Burgess, D. E., 1973. *Proc. Symp. on Television Type Sensors,* p. 21, eds Glaspey, J. W. & Walker, G. A. H., held in University of Columbia, Vancouver.

Burenkov, A. N., Voikhanskaya, N. F. & Rylov, V. S., 1980. *Bull. Spec. Astrophys. Obs. – North Caucasus,* **11**, 58.

Butcher, H. R., 1971. *Proc. astr. Soc. Australia,* **25**, 5.

Butcher, H. R., 1975. *Astrophys. J.*, **199**, 710.

Chaffee, F. H. & Peters, J. R., 1983. *A Pictorial Atlas of the Emission Line Spectrum of a Thorium–Argon Hollow Cathode Lamp,* Whipple Observatory Publication (April).
Courtès, G., 1960. *Annls d'Astrophys.,* **23**, 115.
Learner, R. C. M., 1972. *Auxiliary Instrumentation for Large Telescopes, ESO/CERN Conference,* p. 131, eds Lansten & Reiz.
Macleod, H. A., 1969. *Thin Film Optical Filters,* Adam Hilger Ltd, London.
Meaburn, J., 1973. *Appl. Opt.,* **12**, 2869.
Meaburn, J., 1975. *Appl. Opt.,* **14**, 465.
Meaburn, J., 1980. *Mon. Not. R. astr. Soc.,* **192**, 365.
Meaburn, J. & White, N. J., 1982. *Astrophys. Space Sci.,* **82**, 423.
Meaburn, J. & McMullan, D. E., 1976. *Mon. Not. R. astr. Soc.,* 177, 11.
Palmer, D. R. & Gietzen, J. W., 1972. *Auxiliary Instrumentation for Large Telescopes, ESO/CERN Conference,* p. 111, eds Lansten & Reiz.
Schroeder, D. J. & Anderson, C. M., 1971. *Publs astr. Soc. Pacif.,* **83**, 438.
Taylor, K. & Atherton, P. D., 1980. *Mon. Not. R. astr. Soc.,* **191**, 675.
Wallace, P., 1983. *ASPECT Users' Guide,* Anglo-Australian Obs. Publ.
Wilson, O. C., Münch, G., Flather, E. M. & Coffeen, M. F., 1959. *Astrophys. J. Suppl.,* **4**, 199.
Woolf, N. J., 1959. *PhD thesis,* University of Manchester.
Yeaple, F., 1979. *Product Engineering,* 39 (August).